Environmental Science and Pollution Research (2021) 28:21799–21811
https://doi.org/10.1007/s11356-020-12253-2

RESEARCH ARTICLE

ZnO nanorods/Fe_3O_4-graphene oxide/metal-organic framework nanocomposite: recyclable and robust photocatalyst for degradation of pharmaceutical pollutants

Li Chen[1] · Jun Peng[2] · Fangqi Wang[1] · Donghao Liu[1,3] · Wenrong Ma[1] · Jinmeng Zhang[2] · Wenqing Hu[2] · Ning Li[2] · Pierre Dramou[1,3] · Hua He[1,3,4]

Received: 21 July 2020 / Accepted: 26 December 2020 / Published online: 7 January 2021

Abstract

Nanosized semiconductors are widely utilized as solar energy based photocatalyst. However, the deficiencies such as poor adsorption toward contaminants and recyclability issues, rapid recombination of photo-introduced radicals, and deactivation by scavengers are still be the obstacle. To addressing those obstacles, zeolitic imidazolate framework-8 (ZIF-8), photosensitive ZnO, and paramagnetic Fe_3O_4 were anchored on conductive graphene oxide (GO) to prepare a nanocomposite photocatalyst ZnO/Fe_3O_4-GO/ZIF. The photocatalyst showed good robustness to scavengers of hydroxyl radicals ($OH^{\bullet}$), superoxide radicals ($O_2^{\bullet-}$), and hole (h^+) with hydrophobic ZIF-8 modified surface. Finally, four pharmaceuticals (sulfamethazine, metronidazole, norfloxacin, and 4-acetaminophen) were degraded rapidly under simulated solar irradiation for 1 h, and the photocatalyst could be recycled at least ten times without obvious deactivation. The final results show that combination of semiconductor, graphene oxide and ZIF-8 is a good idea for construction of efficient photocatalyst. It offers new views in interface modification of nanomaterials, photocatalysis, and adsorption.

Keywords Nanosized semiconductor · ZIF-8 · Heterogeneous catalysis · Scavenger · Adsorption

Introduction

The fast demographic growing and the accelerated industrialization lead to scarce water resources drop (Hu et al. 2017; Khetan and Collins 2007). Serious water pollution concerns, including pharmaceuticals and personal care products (PPCPs), are becoming most vital issues of threatening human health and aquatic ecosystems. Among various PPCPs, antibiotics and nonsteroidal anti-inflammatory drugs (NAIDs) are detected worldwide in waters (Liu and Wong 2013; Wang and Wang 2016). Every year, million tons of nitrofurans, sulfonamides, fluoroquinolones and antipyretic analgesics are used in clinic and husbandry, and most of these are transferred into environment and became micropollutants in water (Fatima et al. 2020; Tang et al. 2020). Except acute toxicity, residual of these pharmaceuticals can poison our food and cause drug-resistant strains (Ortiz de Garcia et al. 2013; Ortiz de Garcia et al. 2014). The methods of detection techniques are mainly centered on the solid phase extraction (Daniels et al. 2020) and the analytical techniques (Siddiqui et al. 2017) such as chromatographic, spectroscopic etc. However, none of those methods could directly degrade the target pollutant, thus the

Responsible Editor: Sami Rtimi

Li Chen and Jun Peng equally contributed to this work and should be considered co-first authors.

✉ Pierre Dramou
pierred@cpu.edu.cn

✉ Hua He
dochehua@163.com; jcb_321@163.com

[1] Department of Analytical Chemistry, China Pharmaceutical University, 639 Longmian Avenue, Nanjing 211198, Jiangsu Province, China

[2] The Key Laboratory for Medical Tissue Engineering, College of Medical Engineering, Jining Medical University, Jining 272067, China

[3] Key Laboratory of Biomedical Functional Materials, China Pharmaceutical University, Nanjing 211198, China

[4] Key Laboratory of Drug Quality Control and Pharmacovigilance, Ministry of Education, China Pharmaceutical University, Nanjing 211198, China

photocatalytic technology that integrates detection and degradation has been favored (Majumdar and Pal 2020).

Among various photocatalytic materials, semiconductor-based nanomaterial composites based photocatalysts have gained significant progress in photodegradation of pollutants under sunshine (He and Zhang 2019; Kisch 2013). In the degradation process, photon energy is conversed into chemical energy with migration and reaction of photo-induced electrons/holes. The recombination of photo-generated electron/holes and separation and migration of illumination-induced electrons/holes are key factors for the photocatalytic capability of photocatalysts (Tong et al. 2012; Zhang et al. 2009). Although numerous nanocomposite photocatalysts have been prepared and reported in literature, robust and recyclable photocatalyst with high activities is still important to practical application (Fu et al. 2019). Firstly, the photocatalyst loss is a key obstacle; inefficient recycling of catalyst in economical and useful manners can resulted in relative high cost, secondary contamination and ecotoxicity (Ma et al. 2013; Reiss et al. 2016). Secondly, the recycling issues are the common problem; deactivation often occurred during recycling or complicated regeneration procedures (Alsbaiee et al. 2016; Chalasani and Vasudevan 2013). Thirdly, the poor robustness is the main problem; catalytic activity is mainly affected by coexisting chemicals. Poor endurance of photocatalyst and matrix effect can drive photodegradation uncontrollable and even far from desired outcomes (Chladkova et al. 2015; Van Doorslaer et al. 2012). To improve the above defects, efforts have been made to retard the recombination of charge carriers and modify surface characteristics of photocatalysts for enhanced efficiency (Tong et al. 2012). We prepared a nanocomposite photocatalyst with zeolitic imidazolate framework-8 (ZIF-8), photosensitive ZnO and paramagnetic Fe_3O_4. The combination of semiconductor, graphene oxide, and ZIF-8 offers new views in interface modification of nanomaterials, photocatalysis and adsorption.

Nanosized ZnO is a classic semiconductor with merits such as high photosensitivity, outstanding quantum efficiency, nontoxic nature, and low cost. ZnO is widely applied in photocatalysis and imaging in vivo, whereas its wide implementation is limited by low adsorption capacity, unsatisfactory stability and poor recyclability (Xiong 2013; Xu et al. 2014). Fortunately, the nanosized Fe_3O_4 is famous for its magnetic separation characteristics and excellent recyclability, resulting a widely application in recent years for catalysis, magnetic separation, and intelligent drug delivery. Both of ZnO (bandgap ca. 3.2 eV) (Paul and Balasubramanian 2021) and Fe_3O_4 (with indirect, narrow bandgap) (Liu et al. 2020) can capture energy of photons and give rise to generation of electrons/holes for photodegradation or water splitting. However, recombination of photo-induced electrons/holes is fatal disadvantage for purpose outcomes (Xu et al. 2014) when using ZnO and Fe_3O_4 as photocatalyst. Therefore, a combination of semiconductors and conductors can be considered to prevent charge carriers (Boruah et al. 2017b; Peik-See et al. 2014; Wang et al. 2016a). Graphene oxide (GO) and graphene-based composites have been demonstrated as sorbents or catalyst carriers as its outstanding mechanical properties, high adsorption capacity and high electron mobility (Gadipelli and Guo 2015; Zhang et al. 2005b). However, the aggregation of GO and most nanosized semiconductor materials is easily occurred spontaneously in solution after preparation as their high surface potential energy. The aggregation can reduce specific surface area, bury active sites and reduce recyclability for catalytic application (Wang et al. 2016b; Xu et al. 2018). Metal-organic frameworks (MOFs) are famous for the high surface area with specific functional sites (Yang et al. 2019), and display excellent recyclability with flexible porosity (Feng et al. 2015). In particular, zeolitic imidazolate frameworks-8 (ZIF-8) is an ideal sorbent for separation science (Du et al. 2019; Phan et al. 2010) in MOFs. ZIF-8 is known for high chemical, thermal stability, and high specific area with hydrophobic surface. Thus, a composite photocatalyst was prepared based on ZnO nanorods, Fe_3O_4 nanoparticles, GO, and MOFs for enhanced photocatalytic efficiency.

In photocatalyst ZnO/Fe_3O_4-GO/ZIF, ZnO nanorods and Fe_3O_4 nanoparticles are anchored on GO sheets for efficient photons absorption and fast separation of photo-generated charge carriers (Jeong et al. 2017; Li et al. 2013; Zhan et al. 2013). The paramagnetic Fe_3O_4 can promote the rapid recovery of the catalyst with external magnetic field (Ashour et al. 2017; Hu et al. 2018). Porous ZIF-8 was employed as modification to reinforce adsorption capacity and improve stability of semiconductors. Moreover, ZIF-8 could retard the aggregation of photocatalyst and improve durability and reproducibility. In conclusion, ZnO, Fe_3O_4, GO, and ZIF-8 are complements each other in the final composite photocatalyst ZnO/Fe_3O_4-GO/ZIF. At last, three antibiotics of nitrofurans (metronidazole, MNZ), sulfonamides (sulfamethazine, SMA) and fluoroquinolones (norfloxacin, NFX) and one anti-inflammatory drug (4-acetaminophen, AAP) were chosen to investigate performance of ZnO/Fe_3O_4-GO/ZIF. Total organic carbon in solution was selected to confirm that drugs were decomposed completely or not. Scavengers of hydroxyl radicals ($OH^{\bullet}$), superoxide radicals ($O_2^{\bullet-}$) and hole (h^+) were employed to investigate robustness of ZnO/Fe_3O_4-GO/ZIF. In addition, catalytic performance and synergistic effect of components in ZnO/Fe_3O_4-GO/ZIF were explored carefully.

Experimental section

Materials and instrumentation

Natural graphite flakes (300 mesh, 99.0%) was obtained from Nanjing XFNANO Materials Tech Co., Ltd. (Nanjing,

China). Potassium permanganate ($KMnO_4$, ≥ 99.5%), potassium nitrate (KNO_3, ≥ 99.0%), sulfuric acid (H_2SO_4, 95~98%), phosphoric acid (H_3PO_4, ≥ 85.0%), nitric acid (HNO_3, 65.0~68.0%), hydrochloric acid (HCl, 36.0~38.0%), sodium hydroxide (NaOH, ≥ 96.0%), acetic acid (≥ 99.5%), acetic anhydride (≥ 98.5%), perchloric acid (≥ 99.5%), crystal violet (AR), ethylene glycol (≥ 99.0%), diethylene glycol (≥ 99.0%), $FeCl_3 \cdot 6H_2O$ (99.0%), sodium acetate trihydrate ($CH_3COONa \cdot 3H_2O$, 99%), sodium hydrogen carbonate ($NaHCO_3$, 99.7~100.3%), sodium oxalate (≥ 99.8%), ethylenediaminetetraacetic acid disodium salt (EDTA-2Na, ≥ 99.0%), zinc acetate dehydrate ($Zn(CH_3COO)_2 \cdot 2H_2O$, ≥ 99.0%), zinc nitrate hexahydrate ($Zn(NO_3)_2 \cdot 6H_2O$, ≥ 99.0%), and methanol, ethanol, acetonitrile, and 2-propanol were HPLC grade; all above were purchased from Sinopharm Chemical Reagent Co., Ltd. (Shanghai, China). 2-Methylimidazole (2-MI, 99%) was obtained from Nanjing Chemical Reagent Co Ltd. Ultrapure water was manufactured by EPED-10TH ultra-pure water system (Shanghai precision instrument Co., LTD, Shanghai, China). Nano-ZnO (99.7%, 90 ± 10 nm) was purchased from Klamar Reagents Co., Ltd. (Shanghai, China).

Metronidazole (MNZ, 100%), sulfamethazine (SMA, 99.5%), norfloxacin (NFX, 99.7%), and 4-acetaminophen (AAP, 99.9%) were purchased from National Institutes for Food and Drug Control (Beijing, China).

Other reagents used in present study were purchased from Nanjing Chemical Reagent Co Ltd. (Nanjing, China). All of the reagents were used without further purification. All of the reagents were used without further purification.

SEM and TEM were carried out with S3400N II scanning electron microscope (Hitachi Ltd., Tokyo, Japan) and JEM-200CX Transmission electron microscope (JEOL Ltd., Tokyo, Japan). PXRD was carried out with X"TRA X-ray diffraction (ARL Ltd., Switzerland). FT-IR was tested analyzed by Shimadzu 8400 s Fourier Transform infrared spectroscopy (Shimadzu Ltd., Kyoto, Japan), respectively. VSM was carried out with LS 7307–9309 Vibrating Sample Magnetometer (Lakeshore Ltd., USA). NOVA4000e (Quantachrome Instruments, USA) system and Hitachi U3900 spectrophotometer (Hitachi Ltd., Tokyo, Japan) were used for BET analysis and UV-vis diffuse reflectance spectra, respectively. The xenon light was PLS-SXE300 (output 50 W, 300~2500 nm, facula diameter 30~63 nm, Perfect Light Co Ltd., Beijing, China) for simulative sunshine, and with a UVCUT 400 filter (wavelength ≥ 400 nm) for degradation test under visible light. Shimadzu 20AT HPLC system (two pumps, auto-sampler, column oven and PDA detector) was used for determination of target pollutants before and after degradation. Thermo Scientific™ Hypersil™ ODS C18 column (5 μm, 4.6 × 250 mm) as stationary phase. Injection volume was set as 20 μL, other HPLC conditions for each compound as shown in Table S1. A total organic carbon analyzer (TOC-L, burning at 150 °C, Shimadzu, Kyoto, Japan) was employed for TOC mensuration and analysis. Suitable range: 4 $\mu g \cdot L^{-1}$~30,000 $mg \cdot L^{-1}$.

Synthesis of graphene oxide

Graphene oxide was prepared by modified Hummers' method as literature reports with tiny changes (Becerril et al. 2008; Marcano et al. 2010).

Graphite oxide 3.0 g natural graphite flakes and 5.0 g KNO_3 were placed into a beaker, 30 mL concentration H_3PO_4 was added with continuously stirring and followed by 270 mL concentration H_2SO_4. And an ice-water bath was used for temperature controlling. After for a while, 20 g $KMnO_4$ was added gently and temperature was controlled below 10 °C. Then, the temperature was set at 35 °C for half an hour and 55 °C for 20 h under continuously stirring. Afterward, the reaction was cooled to room temperature, poured onto ice water (250 mL), added 30% H_2O_2 (~ 10 mL) until gas evolution ceased. The color of the mixture turned to yellow. The product was collected by filtration and washed with 10% HCl and ultrapure water for several times before dried in vacuum at 60 °C overnight.

Graphene oxide 2.0 g Graphite oxide was dispersed in 2.0 L ultrapure water, and pH of the solution was adjusted to 10~11 with 20% NaOH solution followed by supersonic treatment for 10 h. Then, centrifugation (10,000 rpm, 5 min) was employed to remove unexfoliated graphite oxide. Upper solution was collected and condensed into ~ 300 mL. Afterward, the graphene oxide was collected by centrifugation (7500 rpm, 10 min) and freeze-drying.

Synthesis of Fe_3O_4-graphene oxide (Fe_3O_4-GO)

The Fe_3O_4-GO nanocomposite was prepared by a solvothermal method (Boruah et al. 2017a; Peng et al. 2018). Specifically, GO (0.2 g) was introduced into a mixture of ethylene glycol (45 mL) and diethylene glycol (45 mL) in 250 mL flask, followed by sonication for 2 h. Then 0.68 g $FeCl_3 \cdot 6H_2O$ was dispersed into the above solution. Subsequently, 4.06 g NaAc and 2.25 g polyethylene glycol were added, followed by stirring for 30 min. Finally, the mixture was sealed in a Teflon-lined stainless-steel autoclave and maintained at 200 °C for 10 h. The product was collected with magnetic field and washed several times with water and ethanol, and dried at 45 °C in a vacuum oven overnight.

Synthesis of ZnO nanorods/Fe_3O_4-GO (ZnO/Fe_3O_4-GO)

ZnO/Fe_3O_4-GO was prepared by two-step aqueous growth method (Wang et al. 2016a; Lv et al. 2015a; Zhang et al. 2005a). Firstly, 150 mg Fe_3O_4-GO was dispersed in 150 mL water, sonication for 20 min and mechanical stirring

(600 rpm) for another 20 min before 0.8 g $Zn(NO_3)_2 \cdot 6H_2O$ added, then pH of the solution was adjusted to 9~10, and maintained under continuously stirring for 1.0 h at room temperature. Subsequently, the product was gathered with a magnet. Secondly, the solid was re-dispersed in 100 mL water and followed by 1.0 g $Zn(CH_3COO)_2 \cdot 2H_2O$ added under stirring. After that, pH was adjusted by NaOH solution to ~ 12; the temperature was set at 80 °C with a water bath and maintained for 1.5 h. Finally, after cooled to room temperature, the ZnO/Fe_3O_4-GO was separated by magnetic field, washed with ethanol and ultrapure water for several times and dried in vacuum at 50 °C.

Synthesis of ZnO/Fe_3O_4-GO/ZIF-8 (ZnO/Fe_3O_4-GO/ZIF)

As high stability and convenient preparation properties of zeolitic imidazolate framework-8 (ZIF-8), ZnO/Fe_3O_4-GO/ZIF was prepared at room temperature in water (Petit and Bandosz 2012; Wang et al. 2016c; Zhan et al. 2013). More concretely, 150 mg ZnO/Fe_3O_4-GO was dispersed into 100 mL water by supersonic treatment for 10 min. Then, 10 mL aqueous solution of $Zn(NO_3)_2 \cdot 6H_2O$ (1.78 g, 6.0 mmol) was added with stirring (500 rpm) in 20 min. Afterwards, 10 mL water solution of 2-methylimidazole (1.23 g, 15 mmol) was added drop by drop with continuously stirring, then pH was adjusted by 20% NaOH solution to ~ 8.0. After reaction for 8 h, the product was isolated with magnetic field and washed with water and ethanol for several times. Finally, the ZnO/Fe_3O_4-GO/ZIF was dried in vacuum at 50 °C for 12 h and calcined at 150 °C under N_2 atmosphere for 2.0 h.

Result and discussion

Synthesis and characterization of ZnO/Fe_3O_4-GO/ZIF

Scheme 1 illustrates the fabrication of the photocatalytic composite ZnO/Fe_3O_4-GO/ZIF. Briefly, Fe_3O_4 nanoparticles were immobilized on GO sheets through a solvothermal method with $FeCl_3$ as iron source (product abbreviated as Fe_3O_4-GO) (Wu et al. 2015). Then, ZnO nanorods were grown on Fe_3O_4-GO in aqueous solutions with two steps of aqueous growth approach (product abbreviated as ZnO/Fe_3O_4-GO/ZIF) (Chang et al. 2011; Wang et al. 2016a). Then, a bottle-around-ship (BAS) method was employed for growth of ZIF-8 on surface of ZnO/Fe_3O_4-GO for preparation of ZnO/Fe_3O_4-GO/ZIF (Zhang et al. 2018).

The morphology of Fe_3O_4-GO, ZnO/Fe_3O_4-GO and ZnO/Fe_3O_4-GO/ZIF was examined by scanning electron microscopy (SEM) and transmission electron microscopy (TEM). As shown in Fig. 1 a and b, GO sheet exhibited an irregular shape and contained some wrinkles, and Fe_3O_4 nanoparticles were anchored onto surface of GO with particle size less than 100 nm, which revealed that graphite was exfoliated successfully during modified Hummers' reaction and ultrasonic treatment. Besides, Fe_3O_4 nanoparticles were immobilized on GO sheet with slight aggregation at wrinkles of GO, which may be attributed to the uniform distribution of functional groups on GO sheets. The images of ZnO/Fe_3O_4-GO are shown in Fig. 1 c and d. ZnO nanorods were grown on Fe_3O_4-GO disorderly with regular cylinder or short rod shape. Like Fe_3O_4 nanoparticles, most ZnO nanorods were grown at wrinkles and defects of GO sheet, which may be owed to functional groups located at edge of GO sheet. There were two kinds of combination of ZnO with Fe_3O_4-GO: one was with Fe_3O_4 nanoparticles, another was with wrinkles of GO sheet (Fig. 1d). What was more, as shown in Fig. 1 e and f, the ZIF-8 was not just simply covered onto ZnO/Fe_3O_4-GO surface, but embedded between GO sheets and become cover of ZnO and Fe_3O_4 nanostructures, which proved that GO is the carrier of ZnO, Fe_3O_4, and ZIF-8, and hybridization of ZIF-8 and GO can create special stacking structure (Fig. 1f).

Powder X-ray diffraction (PXRD) patterns revealed the changes of crystal properties before and after hybridization (Fig. 2a). The strong diffraction peak (2θ) at 10.23 was attributed to the exploited graphite (Fig. 2a, 1) (Liu et al. 2014). All the diffraction peaks (2θ) matched well with data from JCPDS card of Fe_3O_4 and can be assigned to the (111), (220), (311), (400), (422), (511), (440), and (531) of crystal planes of Fe_3O_4 (JCPDS no. 19-0629) (Fig. 2a, 2) (Wang et al. 2013). The diffraction peaks (2θ) at 31.76, 34.4, 36.26, 47.52, 56.62, 62.84, 67.92, and 69.02 were attributed to (100), (002), (101), (102), (110), (103), (112), and (201) of crystal planes of ZnO (JCPDS no. 36-1451) (Fig. 2a, 3) (Le et al. 2017). After covered by ZIF, these distinct diffraction peaks still presented clearly (Fig. 2a, 4) (Chen et al. 2014). Obviously, it can be concluded that Fe_3O_4 and ZnO nanostructure were produced and loaded onto GO sheets.

Moreover, above results were further proved by Fourier transform infrared spectrum (FT-IR) as shown in Fig. 2b. The strong absorption peaks of GO range 400~1400 and 3400~3600 cm^{-1} were weakened by anchoring of Fe_3O_4 nanoparticles (Fig. 2b, 1) (Wu et al. 2015). A broad peak at ~ 580 cm^{-1} was indicated formation of Fe-O bond (Fig. 2b, 2).(Tian et al. 2018) After growth of ZnO nanorods on Fe_3O_4-GO, a new broad peak at ~ 470 cm^{-1} appeared and revealed formation of Zn-O bond. The absorption peak at range 3400~3600 cm^{-1} may be owing to OH group of residual $Zn(OH)_2$ or OH/COOH groups of GO (Fig. 2b, 3) (Sahatiya et al. 2017). After covered by ZIF-8, the distinct absorption peaks of ZIF-8 range 400~1600 cm^{-1} were appeared, and peaks at 3400~3600 cm^{-1} weakened again (Fig. 2b, 4). All above mentioned were proved that the ZnO/Fe_3O_4-GO/ZIF composite was prepared successfully.

For convenient recycling of photocatalyst with external magnetic field, the magnetic susceptibility of Fe_3O_4-GO,

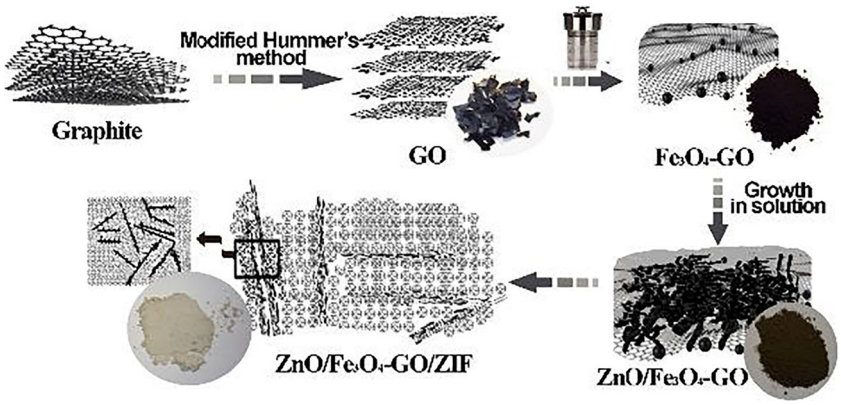

Scheme 1 Process for preparation of ZnO/Fe_3O_4-GO/ZIF nanocomposite

ZnO/Fe_3O_4-GO and ZnO/Fe_3O_4-GO/ZIF was examined by vibrating sample magnetometer (VSM). The results have shown that specific saturation magnetization of Fe_3O_4-GO, ZnO/Fe_3O_4-GO and ZnO/Fe_3O_4-GO/ZIF was 54.9, 38.7 and 21.2 emu g^{-1}, respectively (Fig. 2c). Fe_3O_4-GO, ZnO/Fe_3O_4-GO and ZnO/Fe_3O_4-GO/ZIF were paramagnetic with S-like magnetic hysteresis curves, which show no remanent magnetization or coercivity. With loading of ZnO nanorods, magnetic susceptibility of ZnO/Fe_3O_4-GO was decreased prominently based on that of Fe_3O_4-GO. After covered by porous ZIF-8, further decreasing of magnetic susceptibility was observed (Hu et al. 2018). Because magnetic susceptibility was associated with mass content of Fe_3O_4 in composites, magnetic susceptibility of ZnO/Fe_3O_4-GO and ZnO/Fe_3O_4-GO/ZIF was much lower than that of Fe_3O_4-GO.

As specific surface area and porosity ware most vital characteristics for adsorption and catalysis, nitrogen adsorption–desorption test was employed for investigation of obtained composite photocatalysts. The nitrogen adsorption–desorption isotherms of ZnO/Fe_3O_4-GO and ZnO/Fe_3O_4-GO/ZIF are shown in Fig. 2d. The multipoint Brunauer–Emmett–Teller (BET) specific surface area of ZnO/Fe_3O_4-

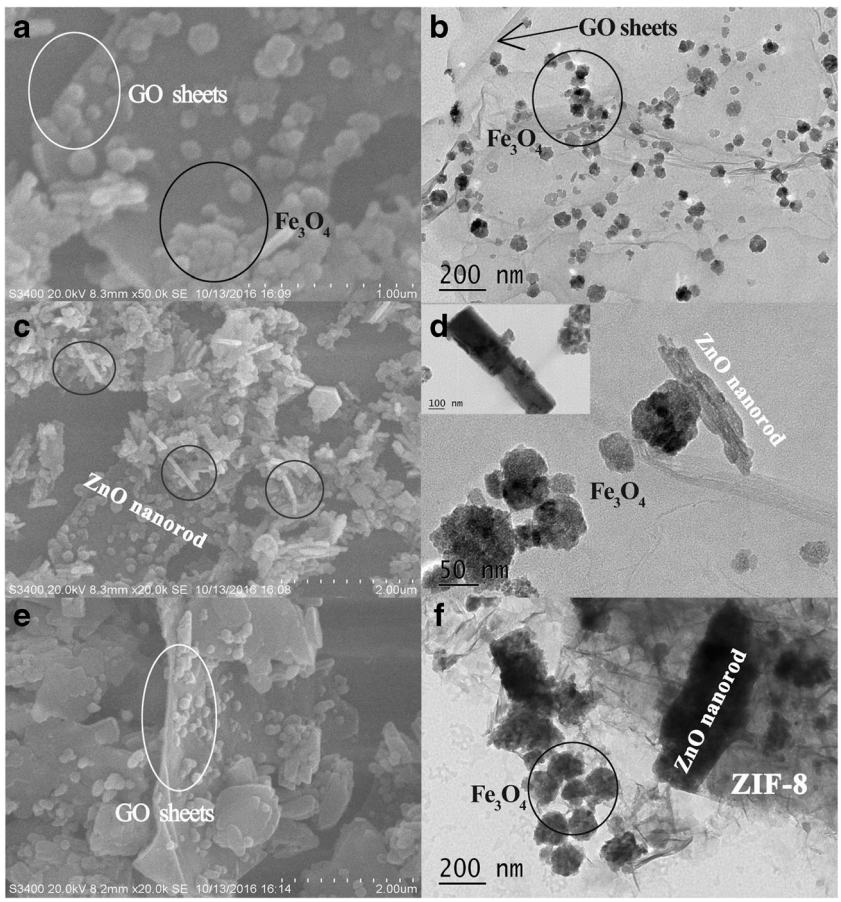

Fig. 1 SEM and TEM photos of Fe_3O_4-GO (a, b), ZnO/Fe_3O_4-GO (c, d) and ZnO/Fe_3O_4-GO/ZIF (e, f) (insert in d: TEM photo of ZnO nanorods)

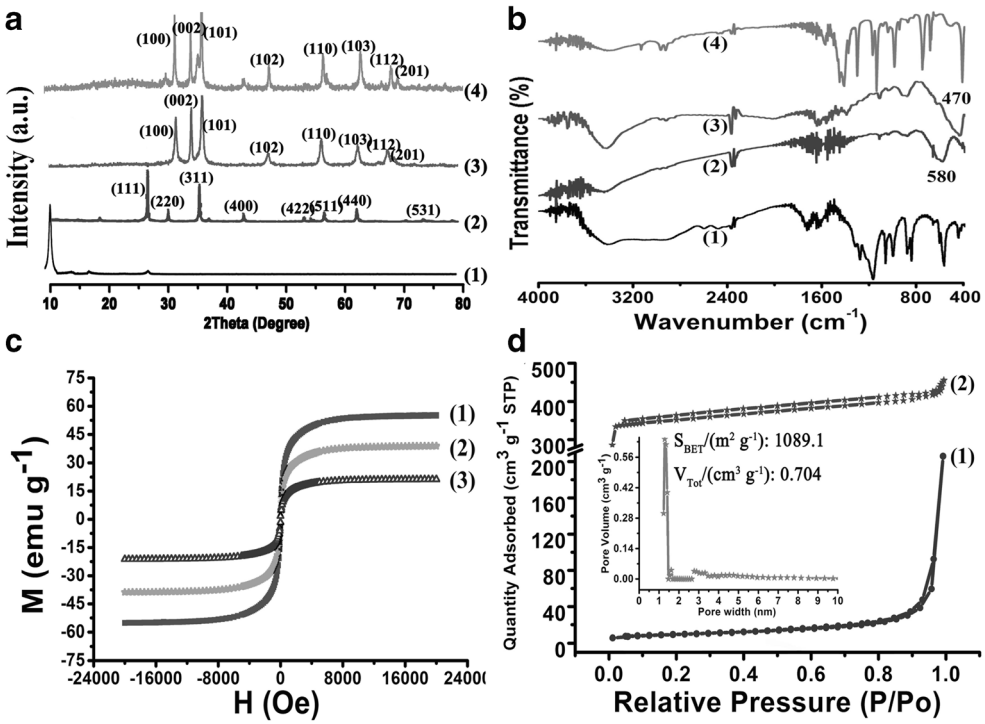

Fig. 2 a PXRD patterns of GO (1), Fe_3O_4-GO (2), ZnO/Fe_3O_4-GO (3), and ZnO/Fe_3O_4-GO/ZIF (4); b FT-IR spectra of GO (1), Fe_3O_4-GO (2), ZnO/Fe_3O_4-GO (3), and ZnO/Fe_3O_4-GO/ZIF (4); c magnetization curves of Fe_3O_4-GO (1), ZnO/Fe_3O_4-GO (2), and ZnO/Fe_3O_4-GO/ZIF (3) (insert showing magnetic separation of ZnO/Fe_3O_4-GO/ZIF in aqueous solution); d N_2 adsorption/desorption isotherms of ZnO/Fe_3O_4-GO (1) and ZnO/Fe_3O_4-GO/ZIF (2) (insert is pore size distribution of ZnO/Fe_3O_4-GO/ZIF)

GO measured to be 36.67 $m^2 \cdot g^{-1}$ (Fig. 2d, 1). This result is much smaller than that of GO and Fe_3O_4-GO reported by literatures (Wu et al. 2015). This has revealed that ZnO grown on Fe_3O_4-GO and reduced the surface area per gram mass. Moreover, the result also has proved that the ZnO/Fe_3O_4-GO is not porous with GO sheets as carrier. On contrary, after combination with ZIF-8, the specific surface area has been enhanced dramatically (Park et al. 2006). The adsorption–desorption isotherms of ZnO/Fe_3O_4-GO/ZIF exhibits Type I property with BET surface area 1089.0 $m^2 \cdot g^{-1}$ and pore volume 0.704 $cm^3 \cdot g^{-1}$ (Fig. 2d, 2). These results may be attributed by new pores formed between ZIF-8 and GO sheets (Kim et al. 2016), which can be proved by that special stacking structure shown in Fig. 1e. In addition, the existence of micro-pores is also confirmed by the pore analysis (as inset figure in Fig. 2d). These have demonstrated that the porosity of final composite can be promoted by combination of GO sheets and ZIF-8. Based on BAS method, Zn^{2+} was contacted and interacted with functional groups of GO before cooperating with organic linkers (2-methylimidazole). After that, ZIF-8 was grown on and between GO sheets with a new kind of pores formed in composite.

Photocatalytic performance

Ultraviolet-visible diffuse reflectance spectra (UV-DR) were employed to explore light absorption of the photocatalyst (Fig. 3a, 1~6). Standard spectrum of sunshine showing that 300~800 nm is the major energy zone of solar light (Fig. 3a, 7). The results of UV-DR showed that absorption of plain ZIF-8 is quite weak (Fig. 3a, 1), and cut-off wavelength of plain ZnO is shorter than 400 nm (Fig. 3a, 2). The broad absorption of Fe_3O_4 and Fe_3O_4-GO have proved that their bandgap is narrower that of plain ZnO (Fig. 3a, 3 and 4). Furthermore, absorption spectrum of ZnO/Fe_3O_4-GO (Fig. 3a, 5) is much broader than that of plain ZnO, which revealed that photons of ultraviolet-visible zone (cut-off wavelength > 600 nm) can be utilized by ZnO/Fe_3O_4-GO. The absorption of Fe_3O_4 and ZnO is enhanced after anchored on GO, indicating that GO can strengthen light absorption of semiconductors. Absorption spectrum of ZnO/Fe_3O_4-GO/ZIF is similar to that of ZnO/Fe_3O_4-GO (Fig. 3a, 6). Namely, compared with ZnO/Fe_3O_4-GO, absorption of ZnO/Fe_3O_4-GO/ZIF is not influenced distinctly by ZIF-8.

Whatever heterogeneous catalysis or removal, adsorption capacity has most important influence on satisfied outcome (Ji et al. 2020; Yan et al. 2020). Adsorption capacities of ZnO/Fe_3O_4-GO/ZIF, Fe_3O_4-GO, ZnO/Fe_3O_4-GO, and nanosized ZnO toward four PPCPs in solutions were investigated and compared carefully. The concentrations of PPCPs were analyzed by HPLC before and after extraction for a certain period (HPLC conditions are listed in Table S1, Electronic Supporting Information: ESI). As shown in Table S2 (ESI), adsorption capacity of ZnO/Fe_3O_4-GO/ZIF was much greater than the other three. Adsorption capacities of Fe_3O_4-GO and ZnO/Fe_3O_4-GO were higher than that of nanosized ZnO. In addition, adsorption performance of Fe_3O_4-GO was better than that of ZnO/Fe_3O_4-GO. According to theory of extraction, adsorption is determined by surface chemistry of sorbent and physiochemical properties of target compounds.

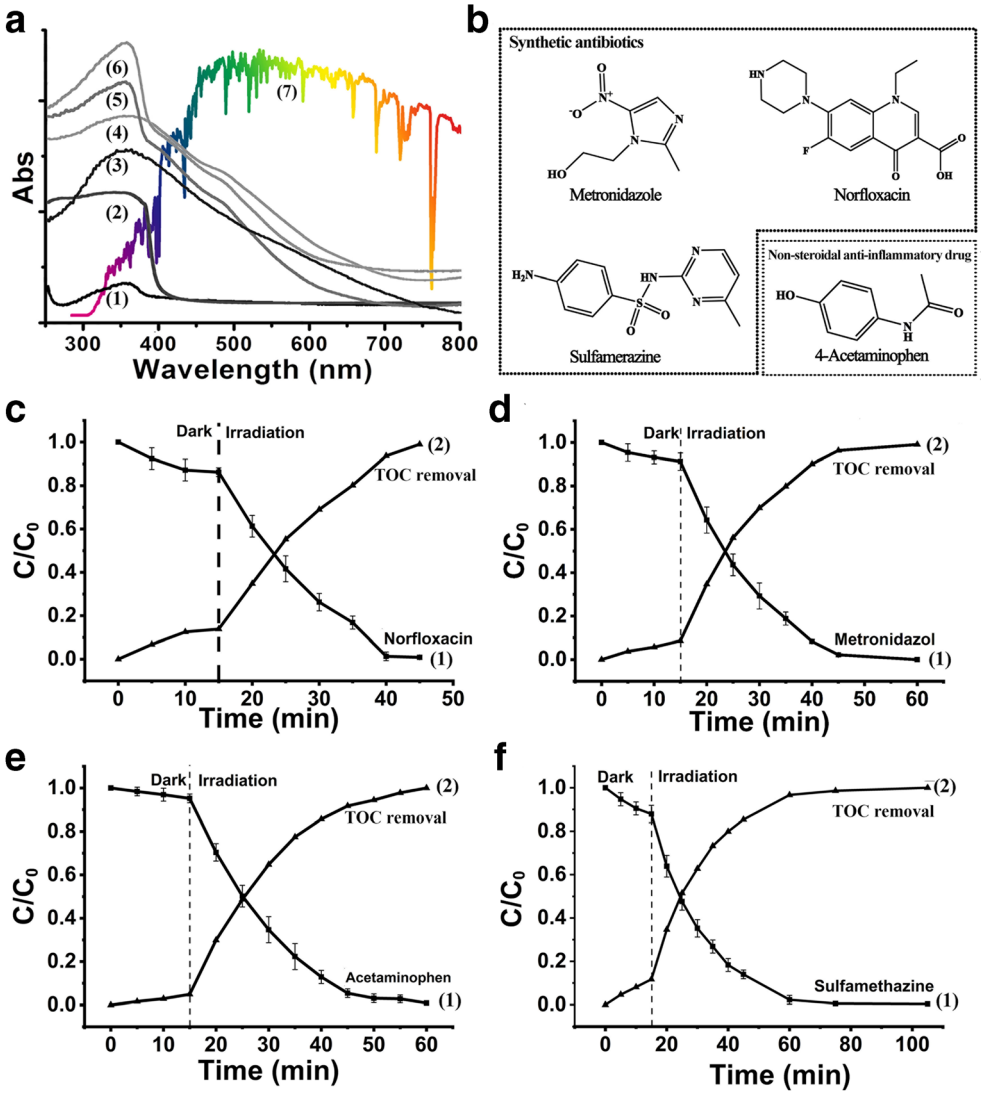

Fig. 3 a UV-vis diffuse reflectance spectra of ZIF-8 (1), commercial nano-ZnO (2), Fe_3O_4 (3), Fe_3O_4-GO (4), ZnO/Fe_3O_4-GO (5), ZnO/Fe_3O_4-GO/ZIF (6), and standard spectrum of sunshine at earth surface (7); b structures of metronidazole (MNZ), sulfamethazine (SMA), norfloxacin (NFX), and 4-acetaminophen (AAP); c degradation curve of NFX (1) and corresponding TOC removal (2); d degradation curve of MNZ (1) and corresponding TOC removal (2); e degradation curve of AAP (1) and corresponding TOC removal (2); f degradation curve of SMA (1) and corresponding TOC removal (2) (C_0: original concentration, 10 ppm; *C*: concentration residual in solution at time *t*)

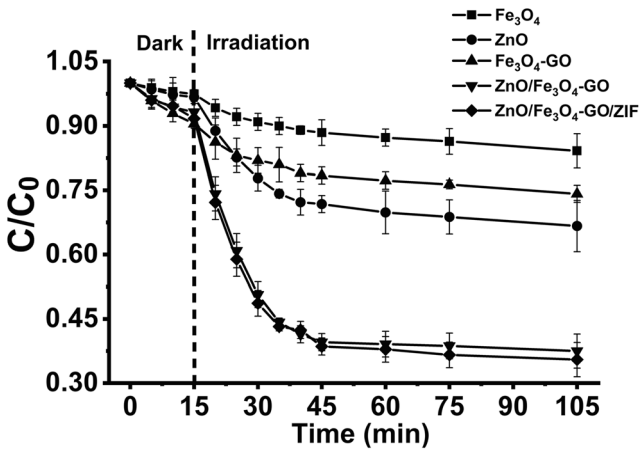

Fig. 4 Photodegradation curves of SMA with Fe_3O_4, nano-ZnO, Fe_3O_4-GO, ZnO/Fe_3O_4-GO, and ZnO/Fe_3O_4-GO/ZIF as catalyst, respectively (C_0: original concentration, 10 ppm; *C*: concentration residual in solution at time t; catalyst dosage: 0.5 $g{\cdot}L^{-1}$)

Compared with ZnO/Fe_3O_4-GO and ZnO/Fe_3O_4-GO/ZIF, ZIF-8 was important to adsorption performance of ZnO/Fe_3O_4-GO/ZIF. For ZnO/Fe_3O_4-GO/ZIF, several interactions, including hydrophobic interaction, π-interaction and van der Waals forces, can force migration of liposoluble chemicals onto the catalyst with its hydrophobic surface of ZIF-8 and unique surface properties of GO.

The photocatalytic performance of ZnO/Fe_3O_4-GO/ZIF was investigated by degradation of opted PPCPs under simulated sunshine irradiation. Concentration decreasing of target pollutants and removal of total organic carbon (TOC) in solution were chosen as criteria for characterization of degradation process. Before irradiation, standing 15 min in dark was employed for establishment of adsorption equilibrium on photocatalyst toward target pollutants. After under irradiation for 45 min, 99.3 ± 0.7% NFX (Fig. 3c, 1), 97.8 ± 1.2% MNZ (Fig. 3d, 1), 99.1 ± 0.7% AAP (Fig. 3e, 1), and 97.7 ± 2.2% SMA (Fig. 3f, 1) were degraded by 0.5 $g{\cdot}L^{-1}$ ZnO/Fe_3O_4-GO/ZIF with

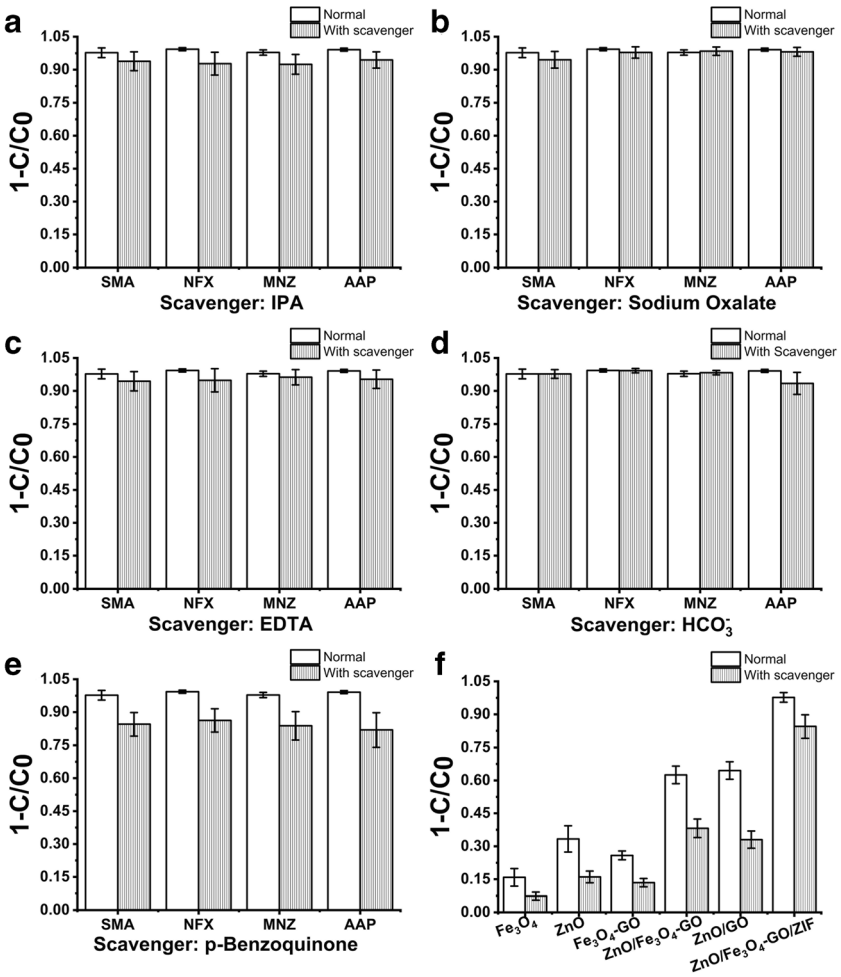

Fig. 5 Degradation outcomes of opted micropollutants with 20 mmol·L^{-1} isopropanol (a), 20 mmol·L^{-1} sodium oxalate (b), 20 mmol·L^{-1} EDTA (c), 20 mmol·L^{-1} HCO_3^- (d), and 6 mmol·L^{-1} p-benzoquinone (d) coexisting as scavenger; photodegradation results of SMA solution with different nanomaterials as catalyst (f) under irradiation for 2 h (original concentration: 10 ppm, catalyst dosage: 0.5 g·L^{-1})

original concentration at 10 ppm level in aqueous solution. After treatment of 60 min, all of these pollutants were almost degraded completely, which revealed that photocatalytic activity of ZnO/Fe_3O_4-GO/ZIF was performed well. Under irradiation, TOC removal was increasing rapidly (Fig. 3, c, d, e, and f). After irradiation of 60 min, TOC residual was decreased close to zero, which proves that these organic pharmaceuticals are decomposed into inorganic carbon compounds, like carbonate or CO_2. The results of TOC removal were consistent with that of above degradation, and clued high catalytic activity of ZnO/Fe_3O_4-GO/ZIF under simulated sunshine. Furthermore, Langmuir-Hinshelwood modeling was utilized for description of heterogeneous photocatalysis with ZnO/Fe_3O_4-GO/ZIF as catalyst (shown in Table S3, ESI). With satisfactory correlation coefficients ($R^2 > 0.95$), pseudo first-order kinetics were conformed to explain degradation of above four micropollutants. The results revealed that adsorption is as important as photoreaction for photodegradation.

In order to investigate photocatalytic performance of each component in the composite photocatalyst, activities of Fe_3O_4, ZnO, Fe_3O_4-GO, ZnO/Fe_3O_4-GO and ZnO/Fe_3O_4-GO/ZIF were explored with degradation of 10 ppm SMA in solution. As shown in Fig. 4, the catalytic activity of composite materials of Fe_3O_4-GO are much higher than single Fe_3O_4, and the same phenomenon is observed between ZnO/Fe_3O_4-GO and ZnO, indicating the high contribution of GO for the first group, and that of both GO and ZnO for the second. The improving catalytic performance of semiconductors due to GO, may be attributed to effective separation of photo-introduced electron/holes and local enrichment of PPCPs because of its unique conductivity and adsorptivity. It is observable that SMA residual in the solution with ZnO/Fe_3O_4-GO as catalyst is higher than that ZnO/Fe_3O_4-GO/ZIF, proving that ZIF-8 sorbent enhances the catalytic activity of semiconductor/GO composite. In addition, compared with Fe_3O_4, Fe_3O_4-GO and ZnO/Fe_3O_4-GO, ZnO and ZnO/GO cannot be separated by magnetic field. Centrifugation or filtration is necessary to separate these two catalysts. Except time-consuming, mass loss is another disadvantage of centrifugation and filtration for recycle. All these outcomes have revealed that high catalytic activity of ZnO/Fe_3O_4-GO/ZIF is derived from absorption of photons by semiconductors, rapid migration of electron/holes by GO, enhanced adsorption of target molecules by GO and ZIF-8, and magnetic separation

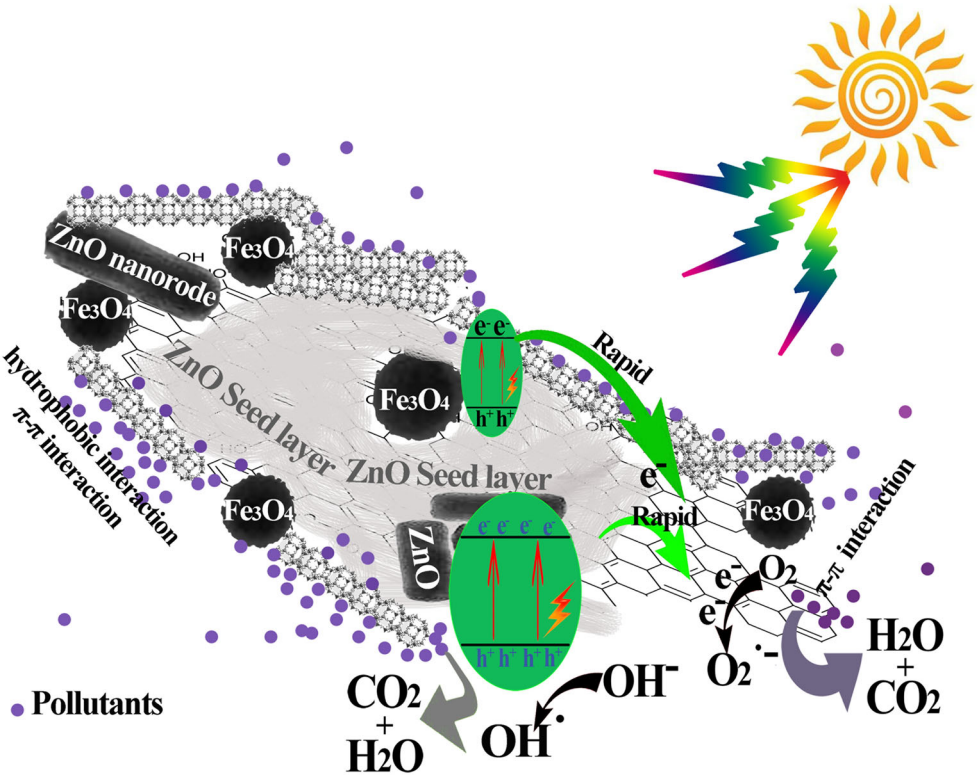

Fig. 6 Photodegradation mechanism of opted micropollutants over ZnO/Fe_3O_4-GO/ZIF under solar irradiation

with paramagnetic Fe_3O_4. First, photons absorbed by ZnO nanorods and Fe_3O_4 provided the energy for oxidation of pollutants. The photocatalytic activities of ZnO nanorods and Fe_3O_4-GO had been widely verified in former literatures (Boruah et al. 2017b; Lv et al. 2015b). Fe_3O_4-GO was used as photocatalyst for degradation under visible irradiation and Fenton-like photodegradation in most cases. Second, the unique conductibility of GO improved the separation and migration of photo-generated electrons. According to former reports (Lv et al. 2015b), the high charge mobility of GO made that it can act as an electron acceptor for the photo-excited electrons from semiconductors, leading to a low charge recombination rate (Zhang et al. 2015). Third, adsorption capacities of ZnO/Fe_3O_4-GO/ZIF to pollutants were enhanced by porous structure and hydrophobic nature of ZIF-8, and this was proved by results of adsorption capacity test. According to catalytic chemistry, achievement of high catalytic activity is depended on rapid adsorption equilibrium. High adsorption capacity is always accompanied by rapid establishment of adsorption equilibrium. Hydrophobic chemistry of ZIF-8 (prepared by reaction of Zn^{2+} with 2-methylimidazole) made that hydrophobic molecules can be adsorbed easily and concentrated locally. In addition, molecular size of most organic pollutants was larger than the pore aperture of ZIF-8 (~3.4 Å), mass transfer and rapid adsorption were enhanced by the surface adsorption. Attributed to the surface adsorption, adsorbed target compounds can access to semiconductors or GO for further oxidation.

Scavenger test

To investigate robustness of the catalyst with scavenger coexist, corresponding scavengers of $OH^{\bullet}$, $O_2^{\bullet-}$ and h^+ were employed for scavenging test, including $NaHCO_3$, isopropanol (IPA), p-benzoquinone, sodium oxalate and ethylenediaminetetraacetic acid (EDTA). In order to avoid mutual interference, individual scavenger was employed for each test. Except scavenger, the other conditions for the investigation were totally as same as former performance test. As shown in Fig. 5 a, b, c, and d, for ZnO/Fe_3O_4-GO/ZIF, no obvious suppression of activity was found with 20 mmol·L^{-1} $NaHCO_3$, oxalate or EDTA as scavenger. Besides, photocatalytic performance of ZnO/Fe_3O_4-GO/ZIF was affected slightly by 6 mmol·L^{-1} of p-benzoquinone (scavenger for $O_2^{\bullet-}$) and 20 mmol·L^{-1} IPA (scavenger for $OH^{\bullet}$) in solution (Fig. 5e). The slight suppression may be caused by the following: (1) scavengers suppress catalytic performance by cleaning up photo-introduced $O_2^{\bullet-}$ and/or $OH^{\bullet}$ radical; (2) competition between target pollution and scavenger occur among catalytic sites on ZnO/Fe_3O_4-GO/ZIF. As hydrophobic surface of ZIF-8, scavenger anions, like EDTA, oxalate and HCO_3^- cannot be enriched nearby or onto the surface of semiconductors and GO sheets, but organic pollutants can be concentrated locally and delivered to reaction sites by ZIF-8 sorbent. On contrary, as π-electron interaction and hydrophobic interaction-based adsorption enhanced by ZIF-8, p-benzoquinone could be absorbed or recruited while pollutant degrading.

Furthermore, IPA could be adsorbed into the aperture of ZIF-8 instead of surface adsorption because of its small size. The results have also proved that $O_2^{\bullet-}$ and $OH^{\bullet}$ radicals were important for photodegradation outcomes. Besides, catalytic robustness of Fe_3O_4, ZnO, Fe_3O_4-GO, ZnO/Fe_3O_4-GO, and ZnO/GO was investigated by 10 ppm SMA with 6 mmol·L^{-1} p-benzoquinone as scavenger. As shown in Fig. 5f, catalytic performance of above five is suppressed significantly by p-benzoquinone. Catalytic robustness of ZnO/Fe_3O_4-GO/ZIF is much greater than that of above five. Without ZIF-8 modification, semiconductors are exposed directly to scavengers. All these results show that ZIF-8 improves catalytic activity and robustness of ZnO/Fe_3O_4-GO/ZIF. In general, ZnO/Fe_3O_4-GO/ZIF is a robust photocatalyst for degradation of opted pharmaceuticals.

Based on all abovementioned results, the degradation mechanism was summarized in Fig. 6. $O_2^{\bullet-}$ and $OH^{\bullet}$ were found to be the vital species for oxidation of pharmaceuticals. Photons were absorbed by photocatalyst, and photo-generated electron/holes were produced. Then, electrons transferred by GO nanosheets were reacted with dissolved O_2 molecules, and $O_2^{\bullet-}$ was produced. Afterwards, $O_2^{\bullet-}$ was reacted with H_2O, and hydroxyl ions (OH^-) were produced. On the other hand, OH^- was reacted with holes, and hydroxyl radicals were produced. At last, adsorbed target micropollutants were oxide by $O_2^{\bullet-}$ and $OH^{\bullet}$ into H_2O, CO_2 and so on. Directly, the results were proved by results of TOC determination in solutions (TOC residual curves are shown in Fig. 3) (Xu et al. 2011).

$$\mathrm{ZnO/Fe_3O_4{-}GO/ZIF} + h\nu = e^-\ (\mathrm{GO}) + h^+\ (\mathrm{ZnO\ or\ Fe_3O_4})$$

$$e^-\ (\mathrm{GO}) + O_2 = O_2^{\bullet-}$$

$$O_2^{\bullet-} + H_2O = OH^-$$

$$OH^- + h^+\ (\mathrm{ZnO\ or\ Fe_3O_4}) = OH^{\bullet}$$

For further verification of stability, the catalytic performance of recovered and regenerated ZnO/Fe_3O_4-GO/ZIF was examined by degradation of 10 ppm SAM. For regeneration, photocatalysts were washed with distilled water, dried in air and followed by slightly grinding. As shown Fig. 7a, in each cycle (standing in dark for 15 min followed by irradiation for 60 min), more than 95% of SMA was degraded. The morphology of reused ZnO/Fe_3O_4-GO/ZIF was examined by TEM and SEM. As shown in Fig. 7, after recycle of 10 times, ZnO nanorods and Fe_3O_4 nanostructures can be observed distinctly and they were connected together tightly (Fig. 7b, c). At same time, wrinkle of GO sheets, ZnO nanorods, Fe_3O_4 nanoparticles and rough surface of ZIF-8 were presented distinctly. As shown in Fig. 7d, ZnO/Fe_3O_4-GO was covered by ZIF-8 nanostructures. ZnO/Fe_3O_4-GO/ZIF was performed as a robust, recyclable and effective catalyst for photodegradation.

Performance under visible light

In order to test catalytic activity of ZnO/Fe_3O_4-GO/ZIF under visible light, a UVCUT 400 filter was utilized to filter UV light from simulated sunshine. As shown in Fig. S1, after standing in dark for 15 min followed by irradiation for 120 min, 37.6 ± 4.0% SMA, 66.1 ± 5.7% NFX, 67.9 ± 3.2% MNZ, and 49.9 ± 3.7% AAP were degraded with ZnO/Fe_3O_4-GO/ZIF as catalyst, which revealed that the visible light can be used by the composite photocatalyst. However, the energy is lower than the simulated sunlight, causing much lower

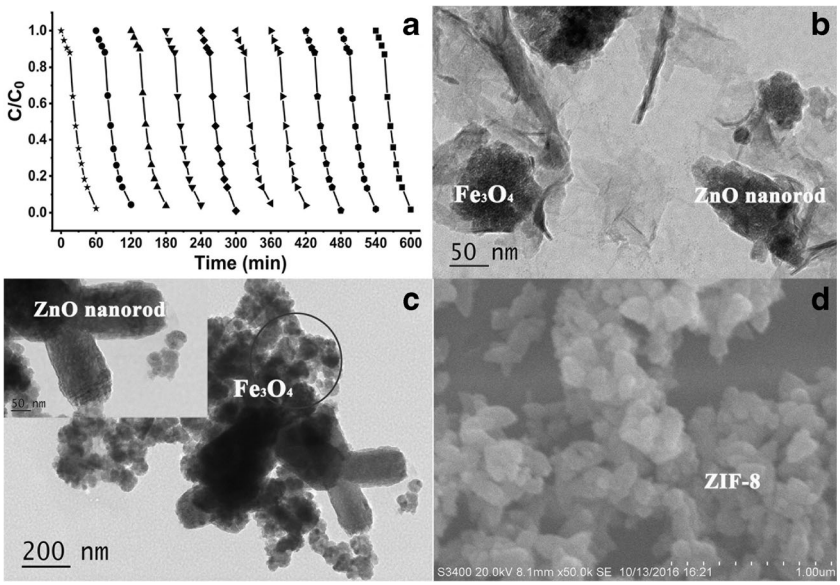

Fig. 7 a photodegradation curves of SMA with reused ZnO/Fe_3O_4-GO/ZIF in ten cycles (C_0: original concentration, 10 ppm; *C*: concentration residual in solution at time t); b, c TEM of ZnO/Fe_3O_4-GO/ZIF after ten cycles; d SEM of ZnO/Fe_3O_4-GO/ZIF after ten cycles

outcomes. In addition, without ZIF-8, photocatalytic activities of ZnO/Fe_3O_4-GO were lower than that of ZnO/Fe_3O_4-GO/ZIF under visible light. The results are also proved by different UV-DR spectra of ZnO/Fe_3O_4-GO/ZIF and ZnO/Fe_3O_4-GO (Fig. 3a).

Conclusions

Based on deliberately design, a composite catalyst was prepared based on ZnO and Fe_3O_4 nanostructures, 2D graphene oxide nanosheets, and hydrophobic metal-organic framework (ZIF-8). Admirable photocatalytic performance of ZnO/Fe_3O_4-GO/ZIF was proved by rapid photodegradation of four pharmaceuticals under simulated sunshine. Compared with commercial catalyst, photocatalytic activity of the photocatalyst was much higher than that of nano-ZnO. This composite catalyst can be reused by mild regeneration for at least 10 times without activity decreasing. Most importantly, compared with naked semiconductors and semiconductors-anchored GO, influence of scavengers on photocatalysis outcomes can be weakened with ZnO/Fe_3O_4-GO/ZIF as catalyst. This study provided a novel strategy for establishment of effective composite photocatalyst: photosensitive "semiconductor" combined with "conductor" and "sorbent." Based on results and phenomenon of this study, catalytic activity under visible light can be enhanced by replace components of ZnO/Fe_3O_4-GO/ZIF in further study, like graphitic C_3N_4 or WO_3 combined with Fe_3O_4-GO and ZIF-8. In addition, other semiconductor-like MOFs also can be utilized to replace ZIF-8 for further improving catalytic performance.

Supplementary Information The online version contains supplementary material available at https://doi.org/10.1007/s11356-020-12253-2.

Authors' contributions Li Chen and Jun Peng are the designers and proponents of this research, responsible for the overall arrangement and completion of the experiment. Besides, they are the writer of the article the article.

Fangqi Wang assisted Li Chen in completing the synthesis of ZnO/Fe_3O_4-GO/ZIF and Photocatalytic performance.

Donghao Liu is responsible for the characterization and the confirmation catalytic activity of ZnO/Fe3O4-GO/ZIF.

Wenrong Ma is responsible for literature review and assisting Donghao Liu to test catalytic activity of ZnO/Fe3O4-GO/ZIF under visible light.

Jinmeng Zhang, Wenqing Hu, and Ning Li assisted Jun Peng in completing the scavenger test.

Pierre Dramou is responsible for experimental guidance and the revision of this manuscript.

Hua He is responsible for research guidance and fund support.

Funding This work was financially supported by the Independent Innovation Fund Project of Agricultural Science and Technology of Jiangsu Province in 2017 (No CX (17)1003), the Guizhou Provincial Science and Technology Department Joint Fund Project (Qian Kehe LH word [2016] No. 7076), the Project Funded by Research Project of Environment Protection Department of Jiangsu Province (Grant No.2015026), Chinese College Students Innovation Project for the R&D of Novel Drugs (J1310032), Chinese College Students Innovation Project for the R&D of Novel Drugs (No. 201910316195), and The National Natural Science Foundation of China (NSFC) under the Category of International (Regional) Cooperation and Exchange Projects (Grant No. 81950410634).

Data availability The datasets used and/or analyzed during the current study are available from the corresponding author on reasonable request.

Compliance with ethical standards

Conflict of interest Not applicable

Ethical approval Not applicable

Consent to participate Not applicable

Competing interests The authors declare that they have no competing interests.

References

Alsbaiee A, Smith BJ, Xiao L, Ling Y, Helbling DE, Dichtel WR (2016) Rapid removal of organic micropollutants from water by a porous beta-cyclodextrin polymer. Nature 529:190-U146 doi:https://doi.org/10.1038/nature16185

Ashour RM et al. (2017) Selective separation of rare earth ions from aqueous solution using functionalized magnetite nanoparticles: kinetic and thermodynamic studies. Chem Eng J 327:286-296 doi:https://doi.org/10.1016/j.cej.2017.06.101

Becerril HA, Mao J, Liu Z, Stoltenberg RM, Bao Z, Chen Y (2008) Evaluation of solution-processed reduced graphene oxide films as transparent conductors. Acs Nano 2:463–470 doi:https://doi.org/10.1021/nn700375n

Boruah PK, Sharma B, Karbhal I, Shelke MV, Das MR (2017a) Ammonia-modified graphene sheets decorated with magnetic Fe3O4 nanoparticles for the photocatalytic and photo-Fenton degradation of phenolic compounds under sunlight irradiation. J Hazard Mater 325:90-100 doi:https://doi.org/10.1016/j.jhazmat.2016.11.023

Boruah PK, Sharma B, Karbhal I, Shelke MV, Das MR (2017b) Ammonia-modified graphene sheets decorated with magnetic Fe_3O_4 nanoparticles for the photocatalytic and photo-Fenton degradation of phenolic compounds under sunlight irradiation. J Hazard Mater 325:90–100. https://doi.org/10.1016/j.jhazmat.2016.11.023

Chalasani R, Vasudevan S (2013) Cyclodextrin-functionalized Fe_3O_4@TiO_2: reusable, magnetic nanoparticles for photocatalytic degradation of endocrine-disrupting chemicals in water supplies. Acs Nano 7:4093–4104 doi:https://doi.org/10.1021/nn400287k

Chang H, Sun Z, Ho KY-F, Tao X, Yan F, Kwok W-M, Zheng Z (2011) A highly sensitive ultraviolet sensor based on a facile in situ solution-grown ZnO nanorod/graphene heterostructure. Nanoscale 3:258–264 doi:https://doi.org/10.1039/c0nr00588f

Chen B, Yang Z, Zhu Y, Xia Y Zeolitic imidazolate framework materials: recent progress in synthesis and applications. J Mater Chem A (2014) 2:16811–16831 doi:https://doi.org/10.1039/c4ta02984d

Chladkova B, Evgenidou E, Kvitek L, Panacek A, Zboril R, Kovar P, Lambropoulou D (2015) Adsorption and photocatalysis of nanocrystalline TiO_2 particles for Reactive Red 195 removal: effect of

humic acids, anions and scavengers. Environ Sci Pollut Res 22: 16514-16524 doi:https://doi.org/10.1007/s11356-015-4806-y

Daniels KD, Park M, Huang Z, Jia A, Flores GS, Lee HK, Snyder SA (2020) A review of extraction methods for the analysis of pharmaceuticals in environmental waters. Crit Rev Environ Sci Technol 50: 2271–2299 doi:https://doi.org/10.1080/10643389.2019.1705723

Du PD, Thanh NVD, Hieu NT (2019) Evaluation of structural properties and catalytic activities in Knoevenagel condensation reaction of zeolitic imidazolate framework-8 synthesized under different conditions. Adv Mater Sci Eng:8 doi:https://doi.org/10.1155/2019/6707143

Fatima S, Asif N, Ahmad R, Fatma T (2020) Toxicity of NSAID drug (paracetamol) to nontarget organism-Nostoc muscorum. Environ Sci Pollut Res 27:35208–35216 doi:https://doi.org/10.1007/s11356-020-09802-0

Feng D, Liu TF, Su J, Bosch M, Wei Z, Wan W, Yuan D, Chen YP, Wang X, Wang K, Lian X, Gu ZY, Park J, Zou X, Zhou HC (2015) Stable metal-organic frameworks containing single-molecule traps for enzyme encapsulation. Nat Commun 6 doi:https://doi.org/10.1038/ncomms6979

Gadipelli S, Guo ZX (2015) Graphene-based materials: synthesis and gas sorption, storage and separation. Prog Mater Sci 69:1-60 doi:https://doi.org/10.1016/j.pmatsci.2014.10.004

He X, Zhang C (2019) Recent advances in structure design for enhancing photocatalysis. J Mater Sci 54:8831–8851 doi:https://doi.org/10.1007/s10853-019-03417-8

Hu Q, Zhao XT, Yang XJ (2017) China's decadal pollution census. Nature 543:491–491 doi:https://doi.org/10.1038/543491d

Hu Y, Mignani S, Majoral J-P, Shen M, Shi X (2018) Construction of iron oxide nanoparticle-based hybrid platforms for tumor imaging and therapy. Chem Soc Rev 47:1874–1900 doi:https://doi.org/10.1039/c7cs00657h

Jeong H, Oh H.M., Gokarna A., Kim H., Yun S.J., Han G.H., Jeong M.S., Lee Y.H., Lerondel G. (2017) Integrated Freestanding Two-dimensional Transition Metal Dichalcogenides. Adv Mater 29 doi:https://doi.org/10.1002/adma.201700308

Ji J, Lu X, Chen C, He M, Huang H (2020) Potassium-modulated delta-MnO2 as robust catalysts for formaldehyde oxidation at room temperature. Appl Catal B-Environ 260 doi:https://doi.org/10.1016/j.apcatb.2019.118210

Khetan SK, Collins TJ (2007) Human pharmaceuticals in the aquatic environment: a challenge to green chemistry. Chem Rev 107: 2319–2364 doi:https://doi.org/10.1021/cr020441w

Kim D, Kim DW, Hong WG, Coskun A (2016) Graphene/ZIF-8 composites with tunable hierarchical porosity and electrical conductivity. J Mater Chem A 4:7710-7717 doi:https://doi.org/10.1039/c6ta01899h

Kisch H (2013) Semiconductor photocatalysismechanistic and synthetic aspects. Angew Chem Int Ed 52:812–847 doi:https://doi.org/10.1002/anie.201201200

Le S, Jiang T, Li Y, Zhao Q, Li Y, Fang W, Gong M (2017) Highly efficient visible-light-driven mesoporous graphitic carbon nitride/ZnO nanocomposite photocatalysts. Appl Catal B-Environ 200: 601–610 doi:https://doi.org/10.1016/j.apcatb.2016.07.027

Li X, Wang Q, Zhao Y, Wu W, Chen J, Meng H (2013) Green synthesis and photo-catalytic performances for ZnO-reduced graphene oxide nanocomposites. J Colloid Interface Sci 411:69–75. https://doi.org/10.1016/j.jcis.2013.08.050

Liu J-L, Wong M-H (2013) Pharmaceuticals and personal care products (PPCPs): a review on environmental contamination in China. Environ Int 59:208-224 doi:https://doi.org/10.1016/j.envint.2013.06.012

Liu J-W, Zhang Y, Chen X-W, Wang J-H (2014) Graphene oxide-rare earth metal-organic framework composites for the selective isolation of hemoglobin. Acs Appl Mater Interfaces 6:10196–10204 doi:https://doi.org/10.1021/am503298v

Liu Q, Zhou L, Liu L, Li J, Wang S, Znad H, Liu S (2020) Magnetic ZnO@Fe3O4 composite for self-generated H2O2 toward photo-Fenton-like oxidation of nitrophenol. Compos Part B 200 doi:https://doi.org/10.1016/j.compositesb.2020.108345

Lv R et al. (2015a) Facile synthesis of ZnO nanorods grown on graphene sheets and its enhanced photocatalytic efficiency. J Chem Technol Biotechnol 90:550-558 doi:https://doi.org/10.1002/jctb.4347

Lv R, Wang X, Lv W, Xu Y, Ge Y, He H, Li G, Wu X, Li X, Li Q (2015b) Facile synthesis of ZnO nanorods grown on graphene sheets and its enhanced photocatalytic efficiency. J Chem Technol Biotechnol 90:550–558. https://doi.org/10.1002/jctb.4347

Ma H, Williams PL, Diamond SA (2013) Ecotoxicity of manufactured ZnO nanoparticles-a review. Environ Pollut 172:76–85 doi:https://doi.org/10.1016/j.envpol.2012.08.011

Majumdar A, Pal A (2020) Recent advancements in visible-light-assisted photocatalytic removal of aqueous pharmaceutical pollutants. Clean Technol Environ Policy 22:11-42 doi:https://doi.org/10.1007/s10098-019-01766-1

Marcano DC, Kosynkin DV, Berlin JM, Sinitskii A, Sun Z, Slesarev A, Alemany LB, Lu W, Tour JM (2010) Improved synthesis of graphene oxide. Acs Nano 4:4806–4814 doi:https://doi.org/10.1021/nn1006368

Ortiz de Garcia S, Pinto Pinto G, Garcia-Encina PA, Irusta Mata R (2013) Ranking of concern, based on environmental indexes, for pharmaceutical and personal care products: an application to the Spanish case. J Environ Manage 129:384–397 doi:https://doi.org/10.1016/j.jenvman.2013.06.035

Ortiz de Garcia SA, Pinto Pinto G, Garcia-Encina PA, Irusta-Mata R (2014) Ecotoxicity and environmental risk assessment of pharmaceuticals and personal care products in aquatic environments and wastewater treatment plants. Ecotoxicology 23:1517–1533 doi:https://doi.org/10.1007/s10646-014-1293-8

Park KS et al. (2006) Exceptional chemical and thermal stability of zeolitic imidazolate frameworks. Proc Natl Acad Sci U S A 103:10186-10191 doi:https://doi.org/10.1073/pnas.0602439103

Paul S, Balasubramanian K (2021) Charge transfer induced excitons and nonlinear optical properties of ZnO/PEDOT:PSS nanocomposite films. Spectrochimica acta Part A, Molecular and biomolecular spectroscopy 245:118901–118901 doi:https://doi.org/10.1016/j.saa.2020.118901

Peik-See T, Pandikumar A, Ngee LH, Huang Nay M, Hua CC (2014) Magnetically separable reduced graphene oxide/iron oxide nanocomposite materials for environmental remediation. Catal Sci Technol 4:4396–4405 doi:https://doi.org/10.1039/c4cy00806e

Peng J, Tian H, Du Q, Hui X, He H (2018) A regenerable sorbent composed of a zeolite imidazolate framework (ZIF-8), Fe3O4 and graphene oxide for enrichment of atorvastatin and simvastatin prior to their determination by HPLC. Microchimica Acta 185 doi:https://doi.org/10.1007/s00604-018-2697-6

Petit C, Bandosz TJ (2012) Exploring the coordination chemistry of MOF-graphite oxide composites and their applications as adsorbents. Dalton Trans 41:4027–4035 doi:https://doi.org/10.1039/c2dt12017h

Phan A, Doonan CJ, Uribe-Romo FJ, Knobler CB, O'Keeffe M, Yaghi OM (2010) Synthesis, structure, and carbon dioxide capture properties of zeolitic imidazolate frameworks. Acc Chem Res 43:58–67 doi:https://doi.org/10.1021/ar900116g

Reiss P, Carriere M, Lincheneau C, Vaure L, Tamang S (2016) Synthesis of semiconductor nanocrystals, focusing on nontoxic and earth-abundant materials. Chem Rev 116:10731–10819 doi:https://doi.org/10.1021/acs.chemrev.6b00116

Sahatiya P, Jones SS, Gomathi PT, Badhulika S (2017) Flexible substrate based 2D ZnO (n)/graphene (p) rectifying junction as enhanced broadband photodetector using strain modulation. 2d Materials 4 doi:https://doi.org/10.1088/2053-1583/aa6534

Siddiqui MR, AlOthman ZA, Rahman N (2017) Analytical techniques in pharmaceutical analysis: a review. Arab J Chem 10:S1409-S1421 doi:https://doi.org/10.1016/j.arabjc.2013.04.016

Tang Y, Huang H, Xue W, Chang Y, Li Y, Guo X, Zhong C (2020) Rigidifying induced fluorescence enhancement in 2D porous covalent triazine framework nanosheets for the simultaneously luminous detection and adsorption removal of antibiotics. Chem Eng J 384 doi:https://doi.org/10.1016/j.cej.2019.123382

Tian H, Peng J, Lv T, Sun C, He H (2018) Preparation and performance study of $MgFe_2O_4$/metal organic framework composite for rapid removal of organic dyes from water. J Solid State Chem 257:40–48. https://doi.org/10.1016/j.jssc.2017.09.017

Tong H, Ouyang S, Bi Y, Umezawa N, Oshikiri M, Ye J (2012) Nano-photocatalytic materials: possibilities and challenges. Adv Mater 24: 229–251 doi:https://doi.org/10.1002/adma.201102752

Van Doorslaer X, Heynderickx PM, Demeestere K, Debevere K, Van Langenhove H, Dewulf J (2012) TiO_2 mediated heterogeneous photocatalytic degradation of moxifloxacin: operational variables and scavenger study. Appl Catal B-Environ 111:150-156 doi:https://doi.org/10.1016/j.apcatb.2011.09.029

Wang JL, Wang SZ (2016) Removal of pharmaceuticals and personal care products (PPCPs) from wastewater: a review. J Environ Manag 182:620–640 doi:https://doi.org/10.1016/j.jenvman.2016.07.049

Wang L, Ji H, Wang S, Kong L, Jiang X, Yang G (2013) Preparation of Fe_3O_4 with high specific surface area and improved capacitance as a supercapacitor. Nanoscale 5:3793-3799 doi:https://doi.org/10.1039/c3nr00256j

Wang K, Xu J, Wang X (2016a) The effects of ZnO morphology on photocatalytic efficiency of ZnO/RGO nanocomposites. Appl Surf Sci 360:270–275 doi:https://doi.org/10.1016/j.apsusc.2015.10.190

Wang M et al. (2016b) The dispersion and aggregation of graphene oxide in aqueous media. Nanoscale 8:14587-14592 doi:https://doi.org/10.1039/c6nr03503e

Wang X et al. (2016c) Rapid construction of ZnO@ZIF-8 heterostructures with size-selective photocatalysis properties. ACS Appl Mater Interfaces 8:9080-9087 doi:https://doi.org/10.1021/acsami.6b00028

Wu J et al. (2015) A nanocomposite consisting of graphene oxide and Fe_3O_4 magnetic nanoparticles for the extraction of flavonoids from tea, wine and urine samples. Microchimica Acta 182:2299-2306 doi:https://doi.org/10.1007/s00604-015-1575-8

Xiong H-M (2013) ZnO nanoparticles applied to bioimaging and drug delivery. Adv Mater 25:5329–5335 doi:https://doi.org/10.1002/adma.201301732

Xu T, Zhang L, Cheng H, Zhu Y (2011) Significantly enhanced photocatalytic performance of ZnO via graphene hybridization and the mechanism study. Appl Catal B-Environ 101:382–387 doi:https://doi.org/10.1016/j.apcatb.2010.10.007

Xu M, Li Q, Fan H (2014) Monodisperse nanostructured Fe_3O_4/ZnO microrods using for waste water treatment. Adv Powder Technol 25:1715-1720 doi:https://doi.org/10.1016/j.apt.2014.06.019

Xu L, Liang H-W, Yang Y, Yu S-H (2018) Stability and reactivity: positive and negative aspects for nanoparticle processing. Chem Rev 118:3209–3250 doi:https://doi.org/10.1021/acs.chemrev.7b00208

Yan T, Liu Q, Wang S, Xu G, Wu M, Chen J, Li J (2020) Promoter rather than inhibitor: phosphorus incorporation accelerates the activity of V2O5-WO3/TiO2 catalyst for selective catalytic reduction of NOx by NH3. Acs Catal 10:2747-2753 doi:https://doi.org/10.1021/acscatal.9b05549

Yang Q, Wang B, Chen Y, Xie YB, Li JR (2019) An anionic In(III)-based metal-organic framework with Lewis basic sites for the selective adsorption and separation of organic cationic dyes. Chin Chem Lett 30:234-238 doi:https://doi.org/10.1016/j.cclet.2018.03.023

Fu Y-s, Li J, Li J (2019) Metal/semiconductor nanocomposites for photocatalysis: fundamentals, structures, applications and properties. Nanomaterials 9 doi:https://doi.org/10.3390/nano9030359

Zhan W-W, Kuang Q, Zhou J-Z, Kong X-J, Xie Z-X, Zheng L-S (2013) Semiconductor@metal-organic framework core-shell heterostructures: a case of ZnO@ZIF-8 nanorods with selective photoelectrochemical response. J Am Chem Soc 135:1926–1933 doi:https://doi.org/10.1021/ja311085e

Zhang H, Yang D, Li D, Ma X, Li S, Que D (2005a) Controllable growth of ZnO microcrystals by a capping-molecule-assisted hydrothermal process. Cryst Growth Des 5:547–550 doi:https://doi.org/10.1021/cg049727f

Zhang YB, Tan YW, Stormer HL, Kim P (2005b) Experimental observation of the quantum Hall effect and Berry's phase in graphene. Nature 438:201–204 doi:https://doi.org/10.1038/nature04235

Zhang H, Chen G, Bahnemann DW (2009) Photoelectrocatalytic materials for environmental applications. J Mater Chem 19:5089–5121. https://doi.org/10.1039/b821991e

Zhang N, Yang M-Q, Liu S, Sun Y, Xu Y-J (2015) Waltzing with the versatile platform of graphene to synthesize composite photocatalysts. Chem Rev 115:10307–10377 doi:https://doi.org/10.1021/acs.chemrev.5b00267

Zhang Y, Li Q, Liu C, Shan X, Chen X, Dai W, Fu X (2018) The promoted effect of a metal-organic frameworks (ZIF-8) on Au/TiO_2 for CO oxidation at room temperature both in dark and under visible light irradiation. Applied Catalysis B-Environmental 224: 283-294 doi:https://doi.org/10.1016/j.apcatb.2017.10.027